An extension of FASTSIM for steady state non-Hertzian contact

Aquib Qazi, Michel Sebès, Hugues Chollet, Honoré Yin, Cédric Pozzolini

An extension of FASTSIM for steady state non-Hertzian contact

Aquib Qazi[1,2,3], Michel Sebès[1], Hugues Chollet[1], Honoré Yin[2], and Cédric Pozzolini[3]

[1] COSYS-GRETTIA, Univ Gustave Eiffel, IFSTTAR, Marne-la-Vallée, France, aquib.qazi@univ-eiffel.fr
[2] Laboratoire Navier, École des Ponts ParisTech, Univ Gustave Eiffel, CNRS, Marne-la-Vallée, France
[3] ESI Group, France

Abstract. The FASTSIM algorithm is widely used in multi-body simulation (MBS) software packages for the evaluation of the tangential wheel-rail contact forces in a steady state. As the algorithm is restricted to Hertzian contact patches, a strip-based local approach is proposed to extend FASTSIM to non-elliptical contact cases. The paper presents this tangential contact approach in detail, which was briefly introduced by Ayasse & Chollet along with the semi-Hertzian method. The contact stresses and their directions are compared with the reference results from the program CONTACT. Different settings for the traction bound are explored to determine their influence on the contact stresses, creep forces, and the limits of the saturation zone in the case of wheel-rail contact. A design of experiments is constructed for a non-Hertzian contact case, with different combinations of the longitudinal, lateral, and spin creepages. The absolute error in the normalised creep forces is used as the quantity of interest and found to be consistent with results in the literature for Hertzian contact cases using FASTSIM.

Keywords: FASTSIM, tangential contact, non-elliptic contact, Hertz, contact stresses

1 Introduction

In multi-body simulation (MBS) codes, the quasi-identity assumption enables the separation of the normal and the tangential wheel-contact problems. The rolling contact problem can then be solved sequentially: the normal contact followed by the tangent one [1]. Several approximate tangential contact approaches have been developed in recent years with the aim of being implemented in MBS software packages. The tangential contact forces are commonly computed with the FASTSIM algorithm [2], assuming a steady state. The simplified theory behind FASTSIM is based on the computation of the coefficients c_{ij} with the help of Kalker's exact linear theory, which are derived from the initial slope of the tangent forces applied on an elliptical contact patch for small creepage values. Other fast methods such as the Vermeulen–Johnson model [3], the

Shen–Hedrick–Elkins model [4], the Book of Tables by Kalker (USETAB) [5], Polach's model [6], and the method FaStrip [7] may also be used. The main drawback for all of the above cited methods is that they remain restricted to elliptical contact patches, although FaStrip has been extended to non-Hertzian patches [8].

Broadly, two approaches may be used to extend FASTSIM type algorithms to non-elliptical contact cases [9]: either by regularising the non-Hertzian contact patch to a single equivalent ellipse, or by extrapolating the original algorithm to a non-elliptic patch [9,10]. An approach based on local strip properties was briefly introduced along with the semi-Hertzian normal contact method in [10], and is further detailed in this paper.

We begin by reviewing the original FASTSIM algorithm based on Kalker's simplified theory [2]. The extension of this algorithm to treat steady state non-Hertzian contact cases is detailed. The tangential stresses, their directions, and the stick-slip division results are presented by considering the contact problem between worn profiles of the wheel-rail pair S1002-UIC60. The obtained results are compared to the reference results from the program CONTACT [11]. The longitudinal, lateral and resultant creep forces are also plotted for a range of values considering the pure spin, pure creepage cases and a combination of all three creepages within a range of realistic values, and similarly compared to CONTACT, before the final conclusions.

2 From FASTSIM over an ellipse to FASTSIM over strips

2.1 The simplified theory

The FASTSIM algorithm based on Kalker's simplified theory [1,2] is perhaps the most widely used method in railway industry codes for evaluating the tangential contact parameters. The idea of the simplified theory is to replace the elastic body by a set of independent springs. Similar to a Winkler foundation, the tangential surface tractions $\boldsymbol{p}$ and the tangential surface displacements $\boldsymbol{u}$ at a given point are assumed to be linearly proportional through a flexibility parameter L. Thus,

$$\boldsymbol{u} = L\boldsymbol{p} \ . \tag{1}$$

In a steady state, the relative slip $\boldsymbol{s}$ is defined as,

$$\boldsymbol{s} = \boldsymbol{w} - \frac{\partial \boldsymbol{u}}{\partial x} \ , \tag{2}$$

with x being the rolling direction in the local reference system. The creepages $\boldsymbol{w}$ at a given point of coordinates $[x,y]$ are defined as,

$$\boldsymbol{w} = [\nu_x - y\varphi \quad \nu_y + x\varphi] \ , \tag{3}$$

where ν_x, ν_y, and φ are the longitudinal, lateral, and spin creepages respectively.

The slip $\boldsymbol{s}$ is first assumed to be zero in Eq. (2) and the adhesion region is supposed to cover the entire contact area. From Eqs. (2) and (3), the longitudinal and lateral displacements u_x and u_y are then given as,

$$u_x = (\nu_x - \varphi y)(x - a_i) \ , \tag{4}$$

$$u_y = \nu_y(x - a_i) + \frac{\varphi}{2}(x^2 - a_i^2) \ , \tag{5}$$

where a_i denotes the half-length of the contact patch at the ith y-coordinate. The contact patch considered in the FASTSIM theory is Hertzian. Integrating the expressions for the displacements over this elliptical contact area $\mathcal{C}$ with semi-axes a and b gives,

$$\iint_{\mathcal{C}} u_x \ dS = -\frac{8}{3}a^2 b\nu_x \ , \tag{6}$$

$$\iint_{\mathcal{C}} u_y \ dS = -\frac{8}{3}a^2 b\nu_y - \frac{\pi}{4}a^3 b\varphi \ . \tag{7}$$

Kalker's linear theory establishes the following expressions for the creep forces in terms of the three creepages,

$$F_x = \iint_{\mathcal{C}} p_x \ dS = -Gabc_{11}\nu_x \ , \tag{8}$$

$$F_y = \iint_{\mathcal{C}} p_y \ dS = -Gabc_{22}\nu_y - G(ab)^{\frac{3}{2}}c_{23}\varphi \ , \tag{9}$$

where G is the modulus of rigidity, and c_{11}, c_{22}, and c_{23} are Kalker's coefficients, which are functions of the Poisson's ratio ν and the ellipse ratio b/a. The linear theory is exact for tiny values of creepages. By multiplying the Eqs. (8) and (9) for the creep forces by the flexibility parameter L, and by comparing them with the Eqs. (1), (6), and (7), we obtain, not one, but instead three expressions for L,

$$L_x = \frac{8a}{3Gc_{11}}, \ L_y = \frac{8a}{3Gc_{22}}, \ L_\varphi = \frac{\pi a\sqrt{a/b}}{4Gc_{23}}. \tag{10}$$

The expressions of the non-saturated shears $\boldsymbol{p}_{ns}$ are given as,

$$p_{x,ns} = -\left(\frac{3}{8}Gc_{11}\nu_x - \frac{4}{\pi}Gc_{23}\sqrt{\frac{b}{a}}y\varphi\right)\left(\frac{a_i - x}{a}\right) \ , \tag{11}$$

$$p_{y,ns} = -\left(\frac{3}{8}Gc_{22}\nu_y\left(\frac{a_i - x}{a}\right) + \frac{2}{\pi}Gc_{23}\sqrt{ab}\varphi\left(\frac{a_i^2 - x^2}{a^2}\right)\right) \ . \tag{12}$$

These expressions correspond to the formulation with three flexibilities given in Eq. (10), although an alternate formulation is also possible using only one flexibility parameter [2]. For the total forces, the use of three flexibilities has been shown to offer better accuracy over using a single flexibility for a range of parameter values (creepages & aspect ratio) that occur for realistic vehicles [12].

In the FASTSIM algorithm, the ellipse is discretised into strips with coordinate y_i, of width δy and length $2a_i$. The ith strip itself is discretised into elements of length δx_i as shown in **Fig. 1**. For each ith strip, the tangential tractions $\boldsymbol{p}$ are deduced iteratively, starting from the leading edge ($j = 0$) where the tractions vanish to zero. The expression for the tractions $\boldsymbol{p}_a$, with adhesion being first assumed at element j, is given by,

$$\boldsymbol{p}_{ij,a} = \boldsymbol{p}_{ij-1} - \delta x_i \frac{\partial \boldsymbol{p}_{ij,ns}}{\partial x} \ . \tag{13}$$

The magnitude of the traction vector $\boldsymbol{p}_{ij}$ at element $[i, j]$ is limited by the traction bound, which is Coulomb's law applied locally,

$$\boldsymbol{p}_{ij} = \boldsymbol{p}_{ij,a} \qquad if \ ||\boldsymbol{p}_{ij,a}|| \leq \mu p_n \ , \tag{14}$$

$$\boldsymbol{p}_{ij} = \frac{\boldsymbol{p}_{ij,a}}{||\boldsymbol{p}_{ij,a}||} \mu p_n \qquad if \ ||\boldsymbol{p}_{ij,a}|| > \mu p_n \ , \tag{15}$$

where μ is the friction coefficient, and p_n is the normal pressure.

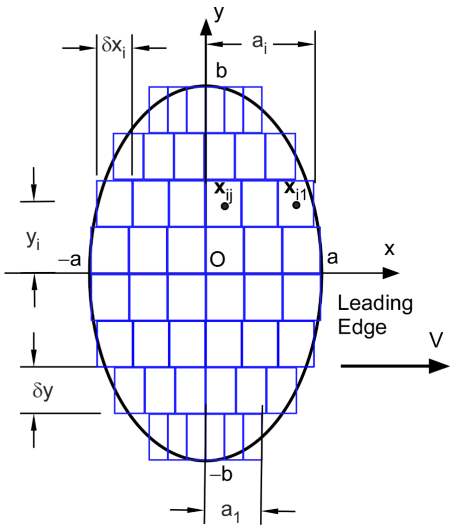

Fig. 1. FASTSIM discretisation

2.2 Extension of FASTSIM for non-Hertzian contact patches

To extend FASTSIM to non-elliptical patches, certain modifications must be introduced in the expressions presented in the previous section. First, the spin term φ associated with the longitudinal creepage ν_x in Eq. (3) vanishes, and the creepages at a given lateral coordinate y_i become,

$$\boldsymbol{w}_i = [\nu_{xi} \quad \nu_{yi} + x\varphi_i] \ , \tag{16}$$

where the subscript i indicates local values for each strip. The neglected term from Eq. (3) accounts for the rolling radius variation, which will be considered in the local expression for the longitudinal creepage ν_{xi}. If the contact angle γ_i does not vary much over the patch, and if the spin creepage is supposed to be purely geometric, the contribution of the spin in the longitudinal component of $\boldsymbol{w}_i$ can be approximated as,

$$y_i\varphi \approx -\frac{y_i \sin\gamma_i}{R_0} = \frac{\delta r_i}{R_0} \ , \tag{17}$$

where R_0 is the rolling radius and δr_i is the rolling radius variation. Subsequently, the local expression for ν_{xi}, as shown in **Fig. 2**, is given as,

$$\nu_{xi} = \nu_x - \frac{\delta r_i}{R_0} \ . \tag{18}$$

The assumption made in Eqs. (16-17) still introduces a slight approximation of the linear theory in the Eqs. (11-12) for non-saturated shears [10].

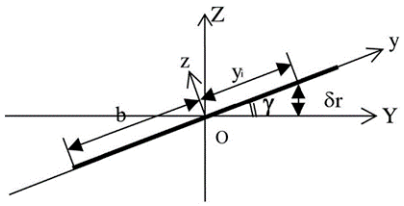

Fig. 2. Description of the longitudinal creepage ν_{xi} for a strip located in y_i.[10]

The spin creepage is supposed to be purely geometric,

$$\varphi_i = -\frac{\sin\gamma_i}{R_0} \ , \tag{19}$$

and the lateral creepage in each strip is similarly given as,

$$\nu_{yi} = \frac{\nu_y}{\cos\gamma_i} \ . \tag{20}$$

The Eqs. (11-12) for non-saturated shears $\boldsymbol{p}_{ns}$ are modified by defining each parameter as a function of local curvatures,

$$p_{x,ns} = -\frac{3}{8} G c_{11i} \nu_{xi} \frac{a_i}{a} \left(\frac{a_i - x}{a_i}\right) \ , \tag{21}$$

$$p_{y,ns} = -\frac{3}{8} G c_{22i} \nu_{yi} \frac{a_i}{a} \left(\frac{a_i - x}{a_i}\right) - \frac{2}{\pi} G c_{23i} \sqrt{\frac{n_i}{m_i}} \varphi_i a_i \frac{a_i}{a} \left(\frac{a_i^2 - x^2}{a_i^2}\right) \ , \tag{22}$$

where m and n denote the Hertzian coefficients for the longitudinal and lateral semi-axes respectively. For non-elliptical patches, the ratio of the longitudinal

semi-axes a_i/a is replaced by a coefficient k_i, between zero and one, whose value is a_i/a in the case of an elliptical patch.

For convenience, the original FASTSIM algorithm is developed using normalised creepages as input, which are defined as the ratio of the non-saturated forces by the Coulomb's limit, both expressed over the ellipse [2]. A similar procedure is used when extending FASTSIM to non-elliptical patches, the difference being that the normalised creepages are expressed for each individual strip. In order to derive the expressions of these entries of FASTSIM, the non-saturated forces $\boldsymbol{F}_{i,ns}$ are deduced from the summation of expressions (21-22) over each strip. Thus,

$$F_{xi,ns} = -\frac{3}{4} G c_{11i} a_i k_i \delta y_i \nu_{xi} \ , \tag{23}$$

$$F_{yi,ns} = -\frac{3}{4} G c_{22i} a_i k_i \delta y_i \nu_{yi} - \frac{8}{3\pi} G c_{23i} a_i^2 k_i \sqrt{\frac{n_i}{m_i}} \delta y_i \varphi_i \ . \tag{24}$$

The normalised forces $\boldsymbol{f}_{i,ns}$, and the associated normalised creepages A_{xi}, A_{yi}, and $A_{\varphi i}$ are finally defined as,

$$f_{xi,ns} = \frac{F_{xi,ns}}{\mu_i N_i} = -A_{xi} \ , \tag{25}$$

$$f_{yi,ns} = \frac{F_{yi,ns}}{\mu_i N_i} = -A_{yi} - A_{\varphi i} \ , \tag{26}$$

where N_i denotes the normal force acting over each strip.

The final adjustment to the original FASTSIM algorithm concerns the choice of the traction bound. Here, several possibilities may be explored: taking the traction bound either as parabolic or semi-ellipsoidal in the longitudinal x direction. According to Hertz theory, p_n is semi-ellipsoidal. However, a parabolic traction bound has been shown to present better results in terms of the division of the stick-slip zones [2,12]. Through some mathematical manipulation, the expression of the normal pressure distribution $p_{n,p}$ corresponding to the choice of a parabolic traction bound in terms of normal force per strip is given as,

$$p_{n,p} = \frac{32}{9\pi} k_i \frac{3}{4} \frac{N_i}{a_i \delta y_i} \left(\frac{a_i^2 - x^2}{a_i^2} \right) \ . \tag{27}$$

Similarly, the expression for the semi-ellipsoidal normal pressure distribution $p_{n,e}$ is given as,

$$p_{n,e} = \frac{2}{\pi} \frac{N_i}{a_i \delta y_i} \sqrt{\frac{a_i^2 - x^2}{a_i^2}} \ . \tag{28}$$

Using a parabolic expression can sometimes lead to cases where the shears exceed the elliptic traction limit, which in turn implies that Coulomb's law is violated. The normalised output from the presented approach are thus weighted using the Hertzian expression to be coherent with Coulomb's theory. The weighing process consists in multiplying the shear stresses obtained using the FASTSIM with a parabolic traction bound by the ratio $p_{n,e}/p_{n,p}$.

3 Results

Worn profiles of wheel-rail pair S1002-UIC60 (1:40) [13], as shown in **Fig. 3**, are chosen to investigate the tangential contact stresses and the stick-slip zone division using the approach described in the previous section. The curvatures are processed following procedure described in [10]. To differentiate the presented method from the original FASTSIM algorithm, the extended method is subsequently referred to as FASTSIM$_{SH}$, where the subscript denotes the idea of the semi-Hertzian approach. The nominal rolling radius is taken as 460 mm. The material properties are those of steel, with the modulus of rigidity $G = 82670$ MPa, and the Poisson's ratio $\nu = 0.27$. The coefficient of friction μ is taken as 0.3. A multi-body simulation of the passenger vehicle from the Manchester Benchmark [14] running on a curved track is used to obtain the steady state input parameters for the FASTSIM$_{SH}$ algorithm. The normal contact force is 64.7 kN. The lateral position of the wheel over the rail $t_y = 5.8$ mm, where a positive value indicates an outward movement of the wheel. The creepage values are taken as $\nu_x = 0.58$ ‰, $\nu_y = 0.061$ ‰, and $\varphi = 0.274$ m^{-1}, with the origin located at the point of geometrical contact.

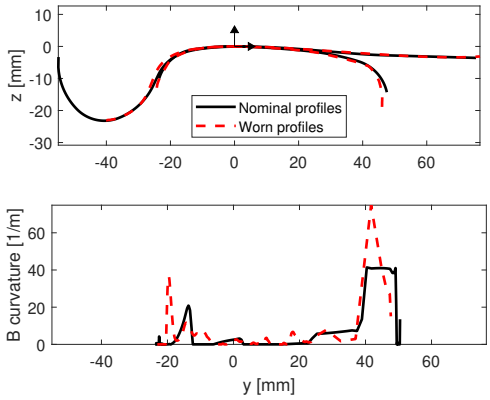

Fig. 3. Nominal and worn profiles described in the tangent plane (top) and the lateral B curvature (bottom) for the wheel-rail pair S1002-UIC60 at position $t_y = 5.8$ mm

The results are validated using the program CONTACT [11], which is based on Kalker's complete theory [1] for the contact between two elastic half-spaces. The normal contact results for the considered wheel position and normal contact force using CONTACT, the semi-Hertzian approach from [10], and the Hertzian theory are presented in **Fig. 4**.

The tangential stresses, their directions and the stick-slip zone division using the various available options are presented in **Fig. 5**. The advantage of using a parabolic traction bound as opposed to a semi-ellipsoidal one is clear, which is also consistent with the results obtained by Kalker [2] and Vollebregt [12]. Nev-

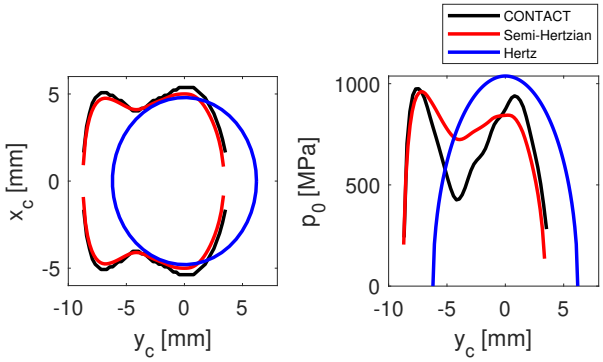

Fig. 4. Contact area (left), and the maximum normal pressure distribution at $x_c = 0$ mm (right) for the wheel position $t_y = 0$ mm.

ertheless, as stated previously, the parabolic traction bound sometimes results in cases where the tractions exceed Coulomb's limit. The weighted parabolic traction bound ensures that the condition $\frac{\max(\boldsymbol{p})}{\mu p_n} \leq 1$ is verified for all cases. The contact stresses and directions using the weighted parabolic setting can be observed to be in a relatively good agreement with the reference results obtained using CONTACT. The presented approach also provides an adequate estimation of the stick and slip zones, which is denoted using the solid line.

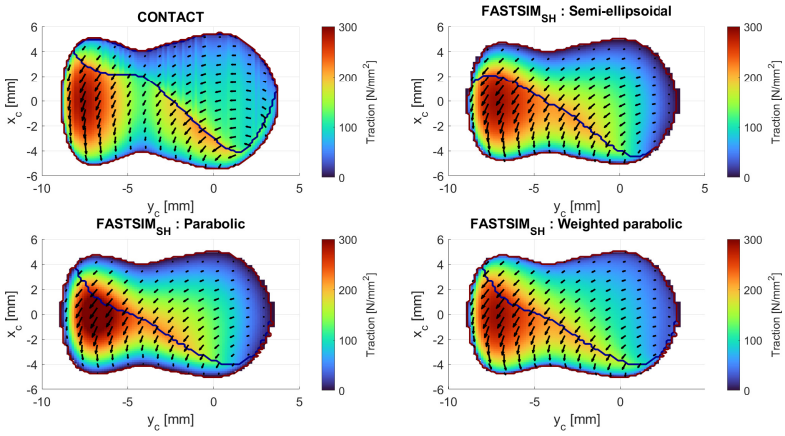

Fig. 5. Tangential tractions, their directions, and the stick-slip zone division. From top left, in clockwise direction: 1) CONTACT, 2) FASTSIM$_{SH}$ with semi-ellipsoidal traction bound, 3) FASTSIM$_{SH}$ with weighted parabolic traction bound, and 4) FASTSIM$_{SH}$ with parabolic traction bound.

In MBS codes, the creep forces rather than the contact stresses are used during online vehicle dynamics simulations. The original FASTSIM algorithm provides a good fast estimation of the tangent forces, which is one of the reasons for its popularity. To evaluate the performance of extended FASTSIM$_{SH}$ algorithm, the creep forces are evaluated for a range of values of the creepages, considering the case of pure spin, where $\nu_x = \nu_y = 0$, and pure creepage, where $\nu_x = \nu_y$ and $\varphi = 0$. As the normal contact results when using the S1002-UIC60 vary considerably for small variations of the wheel position t_y (e.g. see the comparison of normal wheel-rail contact methods in [15]), we restrict ourselves to the contact patches presented in **Fig. 4** to focus on the behaviour of the tangential contact algorithm. The results are presented in Fig. 6 and Fig. 7 respectively, using the setting of a weighted parabolic traction bound for the FASTSIM$_{SH}$ algorithm. The FASTSIM results are calculated using the Hertzian solution at the geometrical contact point. The comparison is not entirely fair in the pure spin case because in FASTSIM, the origin is at the centre of the contact ellipse, which is the same as the pressure centre of gravity, leading to zero F_x. On the contrary, in FASTSIM$_{SH}$ the origin is not at the pressure centre of gravity. It is also possible to take into account this shift of origin with FASTSIM in Eq. (3) [16], however as the general comparison in this study is made with respect to the original algorithm [2], we do not opt for this choice.

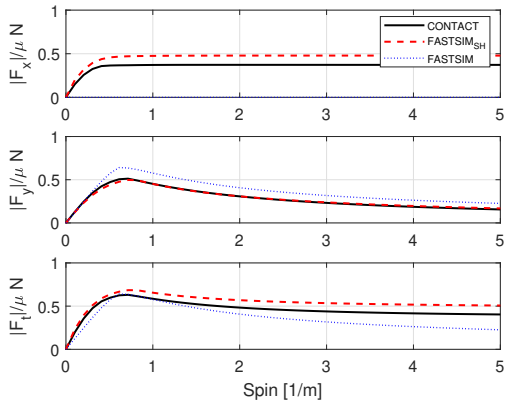

Fig. 6. Normalised creep forces: pure spin ($\nu_x = \nu_y = 0$)

In the pure spin case (**Fig. 6**), the normalised longitudinal creep forces $|F_x|/\mu N$, denoted as f_x, computed using FASTSIM$_{SH}$ can be observed to be slightly overestimated for higher values of the spin creepage. This isn't surprising and may be attributed to the assumption made in Eqs. (16-17). The normalised lateral creep forces can be seen to be in good agreement with the reference results, although the FASTSIM algorithm leads to an overestimation in this case. The creep forces in the pure creepage setting (**Fig. 7**) are generally observed to be in better agreement with the CONTACT results for both algorithms.

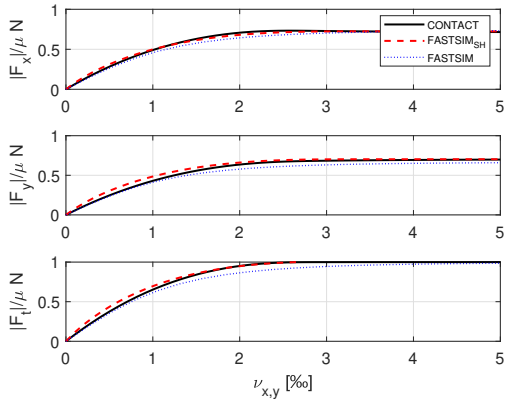

Fig. 7. Normalised creep forces: pure creepage ($\nu_x = \nu_y$, $\varphi = 0$)

As the pure spin and pure creepage cases are largely theoretical, we can additionally consider a combination of all three creepages within a range of realistic values. The longitudinal and lateral creepages are assumed to vary between 0 to 2 ‰, and the spin creepage from 0 to 2 m^{-1}. In the statistical studies presented in [17] and [12] for Hertzian contact patches, the ellipse ratio is considered as an additional varying parameter. Introducing a contact patch parameter in a non-Hertzian case is not so simple, where the normal contact results differ considerably depending on the method that is used [15], and is therefore not considered in this study. A design of experiments is constructed with 8000 simulations, using the FASTSIM$_{SH}$ algorithm with both the semi-ellipsoidal and weighted parabolic traction bounds, and the program CONTACT for different combinations of the creepages acting on the contact patches presented in **Fig. 5**. The normalised creep forces are presented in **Fig. 8**.

The absolute error in the normalised creep forces with respect to CONTACT $|f_{x,y}^{FASTSIM_{SH}} - f_{x,y}^{CONTACT}|$ is used as the quantity of interest to be assessed, and is presented in **Fig. 9** as a function of the percentage of the total tested cases. The absolute error is found to be less than approximately 0.1 in all the cases. For the normalised lateral contact forces f_y, this reduces to below 0.04 for 80% of the tested cases. For the normalised longitudinal contact forces f_x, the absolute error is comparatively higher and reduces to below 0.06 for around 30% of the tested cases. The weighted parabolic traction bound can also be observed to offer a better representation of the creep forces as compared to the semi-ellipsoidal traction bound.

4 Conclusion

The FASTSIM algorithm has been adapted to be used in the case of steady state non-Hertzian contact by using the local geometric properties of the interacting bodies. The paper addresses the fine details of this extrapolation by using the

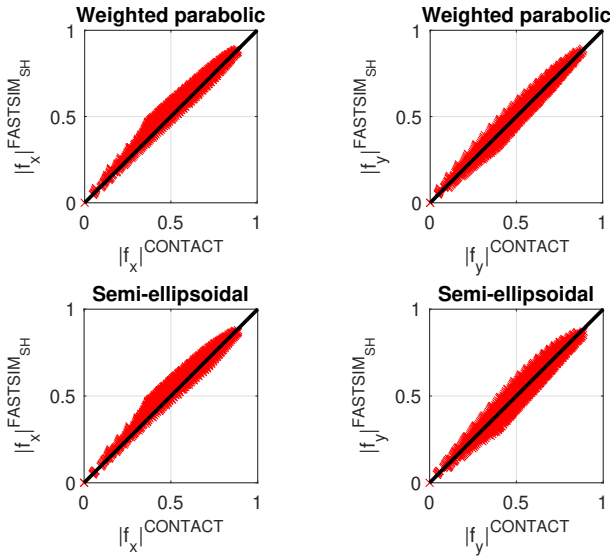

Fig. 8. Comparison of the normalised contact forces computed with the FASTSIM$_{SH}$ algorithm w.r.t. CONTACT

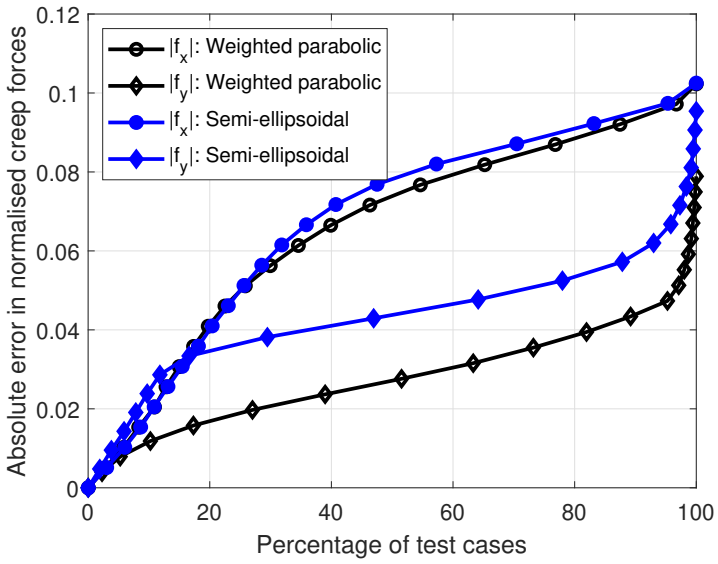

Fig. 9. Absolute error in the normalised contact forces computed with the FASTSIM$_{SH}$ algorithm w.r.t. CONTACT

so called FASTSIM$_{SH}$ algorithm, which was first presented by Ayasse & Chollet in [10]. The results are presented by comparing the tangential tractions, their directions, and the stick-slip zone division with the fully detailed method used in the program CONTACT [11], for a non-elliptical wheel-rail contact case. The influence of the choice of traction bound is investigated, and the parabolic traction bound is shown to provide a better representation of the stick-slip zone, which is in accordance with the previous studies in [2,12]. However, as the parabolic traction bound may sometimes lead to cases where the Coulomb's law is violated, a weighted parabolic traction bound is used in the presented results.

The longitudinal and lateral forces are plotted for a range of creepage values, considering the pure spin and pure creepage conditions. A design of experiment has been constructed using 8000 simulations for different combinations of the three creepages. The absolute error in the normalised creep forces, as compared to the CONTACT results, is used as the quantity of interest. The error in normalised creep forces is found to be less than approximately 0.1 for all the simulations in the considered non-Hertzian contact case, which seems to agree relatively well with the performance of FASTSIM algorithm for Hertzian contact cases [12]. When considering the lateral creep forces, this error drops to below 0.04 for around 80% of the tested cases, while the same is true for around 20% of the longitudinal creep force values.

From the point of view of implementation in MBS codes, the FASTSIM$_{SH}$ method provides a relatively straightforward approach, with the global parameters used in the original FASTSIM approach replaced by their local values. As the basic principle remains more or less the same, FASTSIM$_{SH}$ is as fast as the original algorithm. FASTSIM is already widely used in the railway industry, and using the presented method should offer a good procedure for its extension to non-Hertzian contact patches.

References

1. Kalker, J.J.: Rolling contact phenomena: Linear elasticity. In: B. Jacobson, J.J. Kalker (eds.) Rolling Contact Phenomena, pp. 1–84. Springer Vienna, Vienna (2000)
2. Kalker, J.J.: A fast algorithm for the simplified theory of rolling contact. Vehicle System Dynamics **11**(1), 1–13 (1982). DOI 10.1080/00423118208968684
3. Vermeulen, P.J., Johnson, K.L.: Contact of non-spherical elastic bodies transmitting tangential forces. Journal of Applied Mechanics **31**(2), 338–340 (1964). DOI 10.1115/1.3629610
4. Shen, Z.Y., Hedrick, J.K., Elkins, J.A.: A comparison of alternative creep force models for rail vehicle dynamic analysis. Vehicle System Dynamics **12**(1-3), 79–83 (1983). DOI 10.1080/00423118308968725
5. Kalker, J.J.: Book of tables for the Hertzian creep-force law. Delft University of Technology, Delft, The Netherlands (1996)
6. Polach, O.: A fast wheel-rail forces calculation computer code. Vehicle System Dynamics **33**, 728–739 (1999). DOI 10.1080/00423114.1999.12063125
7. Sichani, M.S., Enblom, R., Berg, M.: An alternative to FASTSIM for tangential solution of the wheel–rail contact. Vehicle System Dynamics **54**(6), 748–764 (2016). DOI 10.1080/00423114.2016.1156135

8. Sichani, M.S., Enblom, R., Berg, M.: A fast wheel–rail contact model for application to damage analysis in vehicle dynamics simulation. Wear **366-367**, 123–130 (2016). DOI 10.1016/j.wear.2016.06.015
9. Piotrowski, J., Kik, W.: A simplified model of wheel/rail contact mechanics for non-Hertzian problems and its application in rail vehicle dynamic simulations. Vehicle System Dynamics **46**, 27–48 (2008). DOI 10.1080/00423110701586444
10. Ayasse, J.B., Chollet, H.: Determination of the wheel rail contact patch in semi-Hertzian conditions. Vehicle System Dynamics **43**(3), 161–172 (2005)
11. Vollebregt, E.: User guide for CONTACT, rolling and sliding contact with friction. Technical report 20-01, version "v20.2". Tech. rep., Vtech CMCC (2020)
12. Vollebregt, E.A., Wilders, P.: Fastsim2: A second-order accurate frictional rolling contact algorithm. Computational Mechanics **47**(1), 105–116 (2011). DOI 10.1007/s00466-010-0536-7
13. Shackleton, P., Iwnicki, S.: Comparison of wheel–rail contact codes for railway vehicle simulation: an introduction to the Manchester contact benchmark and initial results. Vehicle System Dynamics **46**(1-2), 129–149 (2008). DOI 10.1080/00423110701790749
14. Iwnicki, S.: Manchester benchmarks for rail vehicle simulation. Vehicle System Dynamics **30**(3-4), 295–313 (1998). DOI 10.1080/00423119808969454
15. Qazi, A., Yin, H., Sebès, M., Chollet, H., Pozzolini, C.: A semi-analytical numerical method for modelling the normal wheel–rail contact. Vehicle System Dynamics **0**(0), 1–19 (2020). DOI 10.1080/00423114.2020.1854319
16. Vollebregt, E.A.H.: Comments on 'the Kalker book of tables for non-Hertzian contact of wheel and rail'. Vehicle System Dynamics **56**(9), 1451–1459 (2018). DOI 10.1080/00423114.2017.1421767
17. Vollebregt, E., Iwnicki, S., Xie, G., Shackleton, P.: Assessing the accuracy of different simplified frictional rolling contact algorithms. Vehicle System Dynamics **50**(1), 1–17 (2012). DOI 10.1080/00423114.2011.552618